Today's outline - April 14, 2020 (part A)

Today's outline - April 14, 2020 (part A)

- Resonant techniques

Today's outline - April 14, 2020 (part A)

- Resonant techniques

Homework Assignment #7:
Chapter 7: 2,3,9,10,11
due Thursday, April 23, 2020

Today's outline - April 14, 2020 (part A)

- Resonant techniques

Homework Assignment #7:
Chapter 7: 2,3,9,10,11
due Thursday, April 23, 2020

Final Exam, Tuesday, May 5, 2020 13:00 CDT

Today's outline - April 14, 2020 (part A)

- Resonant techniques

Homework Assignment #7:
Chapter 7: 2,3,9,10,11
due Thursday, April 23, 2020

Final Exam, Tuesday, May 5, 2020 13:00 CDT

Tell me what time slot you would prefer for your presentation (first come, first served!)

13:00	14:00	15:00	16:00	17:00	18:00
13:20	14:20	15:20	16:20	17:20	18:20
13:40	14:40	15:40	16:40	17:40	18:40

Today's outline - April 14, 2020 (part A)

- Resonant techniques

Homework Assignment #7:
Chapter 7: 2,3,9,10,11
due Thursday, April 23, 2020

Final Exam, Tuesday, May 5, 2020 13:00 CDT

Tell me what time slot you would prefer for your presentation (first come, first served!)

13:00	14:00	15:00	16:00	17:00	18:00
13:20	14:20	15:20	16:20	17:20	18:20
13:40	14:40	15:40	16:40	17:40	18:40

Send me your presentation in Powerpoint or PDF format before the exam

Matrix elements for x-ray-electron interaction

$$\mathcal{H}_I = \frac{e\vec{p}\cdot\vec{A}}{m} + \frac{e^2A^2}{2m},$$

Matrix elements for x-ray-electron interaction

$$\mathcal{H}_I = \frac{e\vec{p}\cdot\vec{A}}{m} + \frac{e^2A^2}{2m}, \qquad \vec{A} = \hat{\varepsilon}\sqrt{\frac{\hbar}{2\epsilon_0 V\omega}}\left[a_k e^{i\vec{k}\cdot\vec{r}} + a_k^\dagger e^{-i\vec{k}\cdot\vec{r}}\right]$$

Matrix elements for x-ray-electron interaction

$$\mathcal{H}_I = \frac{e\vec{p}\cdot\vec{A}}{m} + \frac{e^2 A^2}{2m}, \qquad \vec{A} = \hat{\varepsilon}\sqrt{\frac{\hbar}{2\epsilon_0 V\omega}}\left[a_k e^{i\vec{k}\cdot\vec{r}} + a_k^\dagger e^{-i\vec{k}\cdot\vec{r}}\right]$$

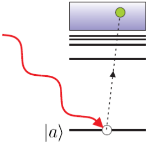

Absorption is a first order process that involves a single photon annihilation operator (a_k) and a core electron promoted to the continuum

Matrix elements for x-ray-electron interaction

$$\mathcal{H}_I = \frac{e\vec{p}\cdot\vec{A}}{m} + \frac{e^2A^2}{2m}, \qquad \vec{A} = \hat{\varepsilon}\sqrt{\frac{\hbar}{2\epsilon_0 V\omega}}\left[a_k e^{i\vec{k}\cdot\vec{r}} + a_k^\dagger e^{-i\vec{k}\cdot\vec{r}}\right]$$

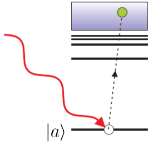

Absorption is a first order process that involves a single photon annihilation operator (a_k) and a core electron promoted to the continuum

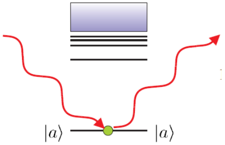

Thomson scattering is a first order process that involves both photon annihilation and creation operators with an electron that remains in its original state

Matrix elements for x-ray-electron interaction

$$\mathcal{H}_I = \frac{e\vec{p}\cdot\vec{A}}{m} + \frac{e^2A^2}{2m}, \qquad \vec{A} = \hat{\varepsilon}\sqrt{\frac{\hbar}{2\epsilon_0 V\omega}}\left[a_k e^{i\vec{k}\cdot\vec{r}} + a_k^\dagger e^{-i\vec{k}\cdot\vec{r}}\right]$$

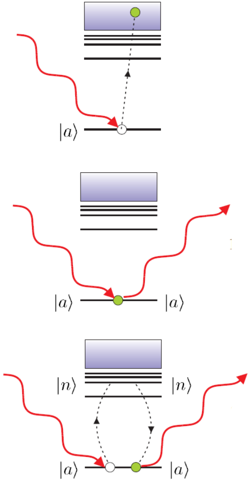

Absorption is a first order process that involves a single photon annihilation operator (a_k) and a core electron promoted to the continuum

Thomson scattering is a first order process that involves both photon annihilation and creation operators with an electron that remains in its original state

Resonant scattering is a second order process that involves photon annihilation and creation operators, a core electron and an intermediate empty electron state

Diffraction anomalous fine structure (DAFS)

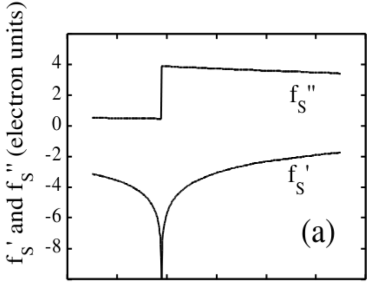

Diffraction anomalous fine structure (DAFS)

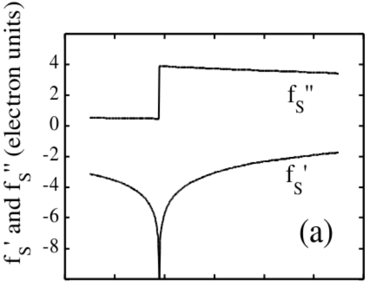

The simple model of resonant scattering and absorption produce a resonance dip in the real part of scattering factor of an atom at the absorption edge but there is no structure in either for an isolated atom

Diffraction anomalous fine structure (DAFS)

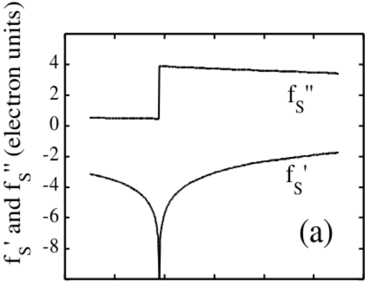

The simple model of resonant scattering and absorption produce a resonance dip in the real part of scattering factor of an atom at the absorption edge but there is no structure in either for an isolated atom

However, an atom in solid or liquid exhibits EXAFS oscillations in the absorption cross section and f'' which are reflected in the resonant term f' as well

Diffraction anomalous fine structure (DAFS)

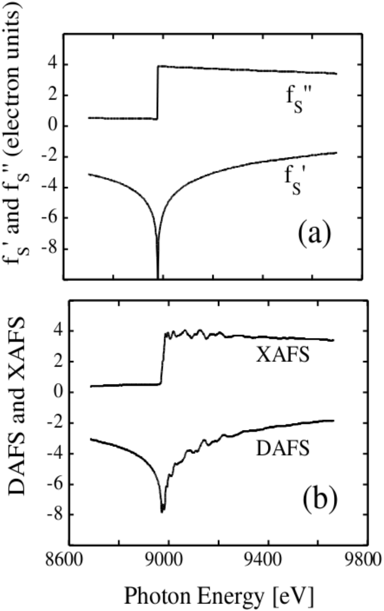

The simple model of resonant scattering and absorption produce a resonance dip in the real part of scattering factor of an atom at the absorption edge but there is no structure in either for an isolated atom

However, an atom in solid or liquid exhibits EXAFS oscillations in the absorption cross section and f'' which are reflected in the resonant term f' as well

Diffraction anomalous fine structure (DAFS)

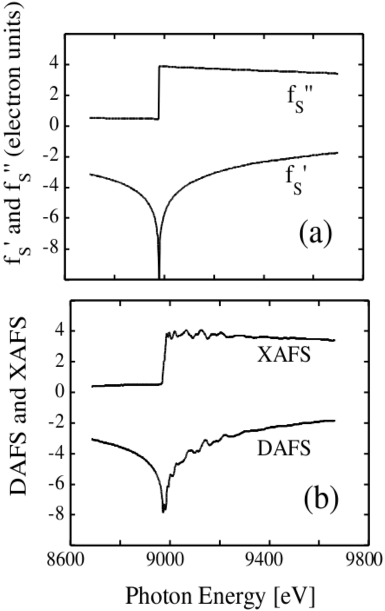

The simple model of resonant scattering and absorption produce a resonance dip in the real part of scattering factor of an atom at the absorption edge but there is no structure in either for an isolated atom

However, an atom in solid or liquid exhibits EXAFS oscillations in the absorption cross section and f'' which are reflected in the resonant term f' as well

These oscillations can be measured in Bragg reflections contributed to by the atom with the absorption edge and exploited to extract site-specific EXAFS

The DAFS experiment

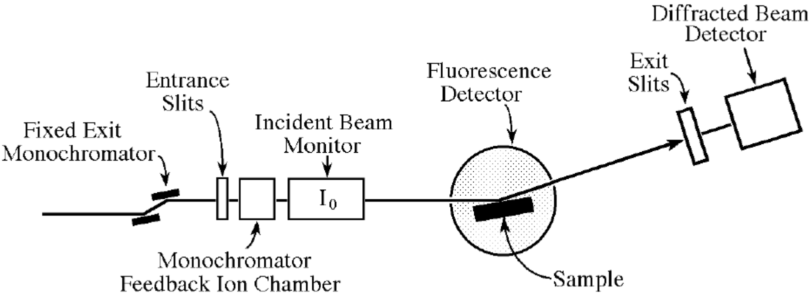

The DAFS experiment

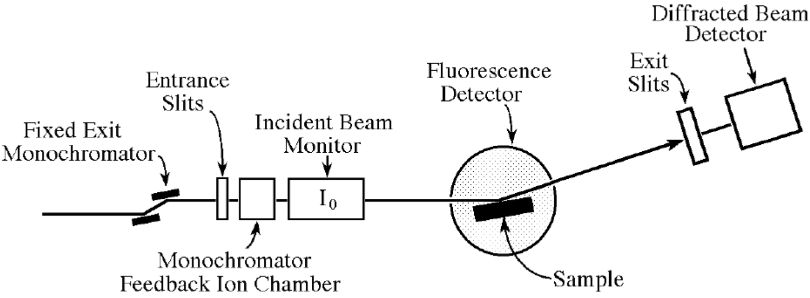

As the energy is swept through the absorption edge, the angle of the sample and the detector are changed to remain in a Bragg condition.

The DAFS experiment

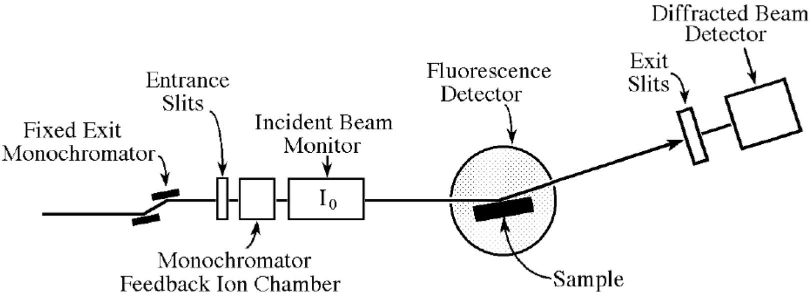

As the energy is swept through the absorption edge, the angle of the sample and the detector are changed to remain in a Bragg condition.

Several peaks are measured to be able to extract information about individual atomic sites.

The DAFS experiment

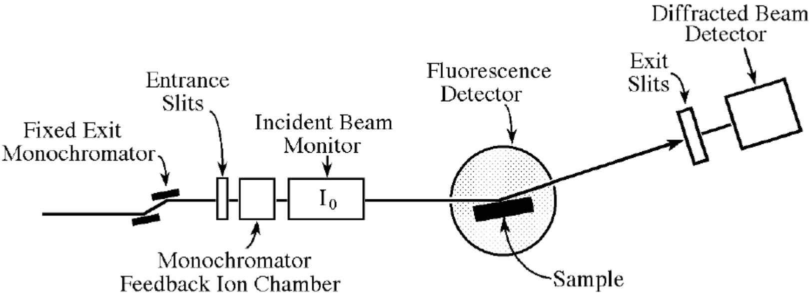

As the energy is swept through the absorption edge, the angle of the sample and the detector are changed to remain in a Bragg condition.

Several peaks are measured to be able to extract information about individual atomic sites.

Initially experiments were done on single crystals but now DAFS on powders can be performed

DAFS of $YBa_2Cu_3O_7$

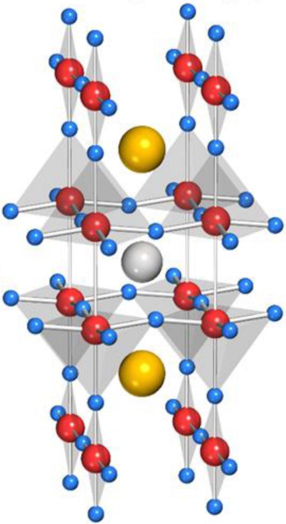

'Separated anomalous scattering amplitudes for the inequivalent Cu sites in $YBa_2Cu_3O_{7-\delta}$ using DAFS," J.O. Cross, M. Newville, L.B. Sorensen, H.J. Straiger, C.E. Bouldin, and J.C. Woicik, *J. Phys.* **C2**, 745-747 (1997).

DAFS of $YBa_2Cu_3O_7$

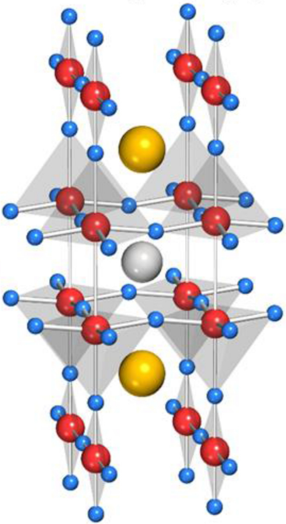

$YBa_2Cu_3O_{7-\delta}$ is a defect perovskite structure with two distinct copper sites

'Separated anomalous scattering amplitudes for the inequivalent Cu sites in $YBa_2Cu_3O_{7-\delta}$ using DAFS," J.O. Cross, M. Newville, L.B. Sorensen, H.J. Straiger, C.E. Bouldin, and J.C. Woicik, *J. Phys.* **C2**, 745-747 (1997).

DAFS of $YBa_2Cu_3O_7$

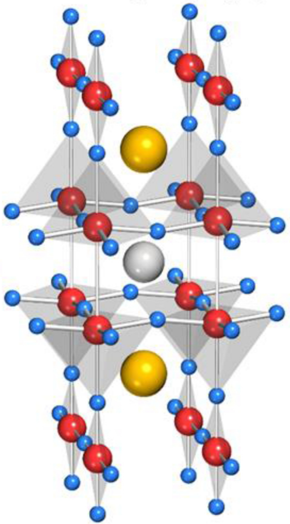

$YBa_2Cu_3O_{7-\delta}$ is a defect perovskite structure with two distinct copper sites

the two Cu sites have distinct local environments, the Cu2 site has square-pyramidal coordination and the Cu1 site has square planar coordination

'Separated anomalous scattering amplitudes for the inequivalent Cu sites in $YBa_2Cu_3O_{7-\delta}$ using DAFS," J.O. Cross, M. Newville, L.B. Sorensen, H.J. Straiger, C.E. Bouldin, and J.C. Woicik, *J. Phys.* **C2**, 745-747 (1997).

DAFS of $YBa_2Cu_3O_7$

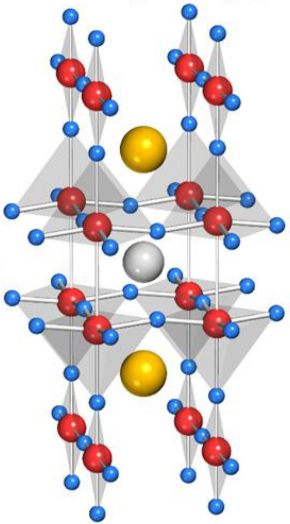

$YBa_2Cu_3O_{7-\delta}$ is a defect perovskite structure with two distinct copper sites

the two Cu sites have distinct local environments, the Cu2 site has square-pyramidal coordination and the Cu1 site has square planar coordination

with simple EXAFS, you will see a superposition of the two sites in a 2:1 ratio

'Separated anomalous scattering amplitudes for the inequivalent Cu sites in $YBa_2Cu_3O_{7-\delta}$ using DAFS," J.O. Cross, M. Newville, L.B. Sorensen, H.J. Straiger, C.E. Bouldin, and J.C. Woicik, *J. Phys.* **C2**, 745-747 (1997).

DAFS of $YBa_2Cu_3O_7$

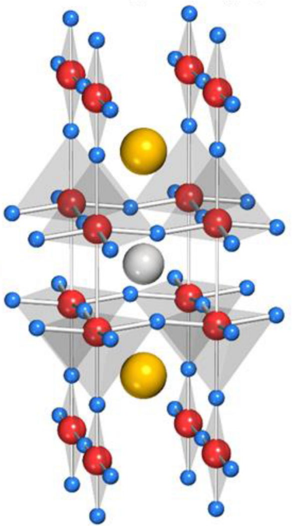

$YBa_2Cu_3O_{7-\delta}$ is a defect perovskite structure with two distinct copper sites

the two Cu sites have distinct local environments, the Cu2 site has square-pyramidal coordination and the Cu1 site has square planar coordination

with simple EXAFS, you will see a superposition of the two sites in a 2:1 ratio

by measuring the DAFS of multiple (00l) diffraction peaks, it is possible to separate the EXAFS of the two Cu sites

'Separated anomalous scattering amplitudes for the inequivalent Cu sites in $YBa_2Cu_3O_{7-\delta}$ using DAFS," J.O. Cross, M. Newville, L.B. Sorensen, H.J. Straiger, C.E. Bouldin, and J.C. Woicik, *J. Phys.* **C2**, 745-747 (1997).

DAFS of $YBa_2Cu_3O_7$

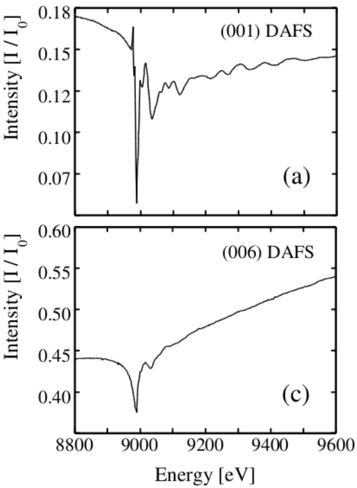

'Separated anomalous scattering amplitudes for the inequivalent Cu sites in $YBa_2Cu_3O_{7-\delta}$ using DAFS," J.O. Cross, M. Newville, L.B. Sorensen, H.J. Straiger, C.E. Bouldin, and J.C. Woicik, *J. Phys.* **C2**, 745-747 (1997).

DAFS of $YBa_2Cu_3O_7$

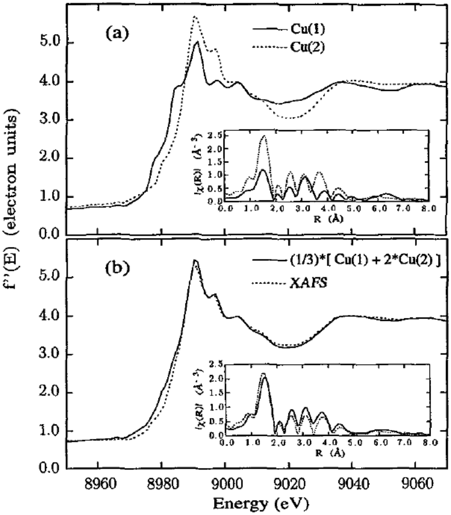

'Separated anomalous scattering amplitudes for the inequivalent Cu sites in $YBa_2Cu_3O_{7-\delta}$ using DAFS," J.O. Cross, M. Newville, L.B. Sorensen, H.J. Straiger, C.E. Bouldin, and J.C. Woicik, *J. Phys.* **C2**, 745-747 (1997).

DAFS of $YBa_2Cu_3O_7$

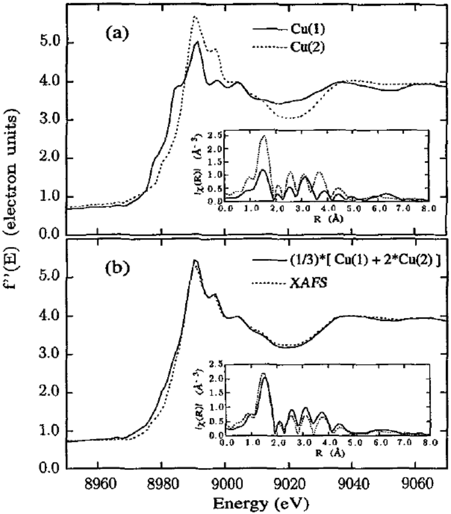

The two Cu sites are distinctly different in both edge position and shape

'Separated anomalous scattering amplitudes for the inequivalent Cu sites in $YBa_2Cu_3O_{7-\delta}$ using DAFS," J.O. Cross, M. Newville, L.B. Sorensen, H.J. Straiger, C.E. Bouldin, and J.C. Woicik, *J. Phys.* **C2**, 745-747 (1997).

DAFS of $YBa_2Cu_3O_7$

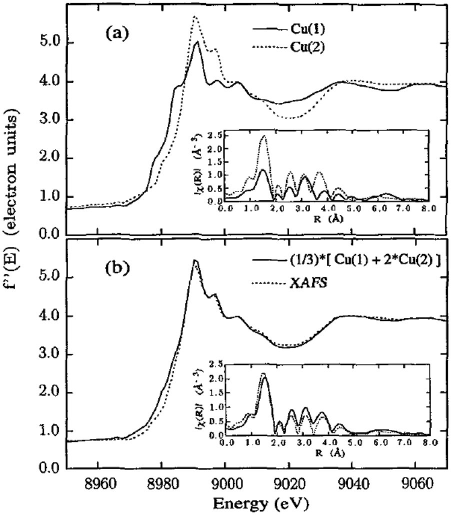

The two Cu sites are distinctly different in both edge position and shape

the Fourier transform is also significantly different for the two sites, particularly the amplitude of the Cu-O peak in the real-space EXAFS

'Separated anomalous scattering amplitudes for the inequivalent Cu sites in $YBa_2Cu_3O_{7-\delta}$ using DAFS," J.O. Cross, M. Newville, L.B. Sorensen, H.J. Straiger, C.E. Bouldin, and J.C. Woicik, *J. Phys.* **C2**, 745-747 (1997).

DAFS of $YBa_2Cu_3O_7$

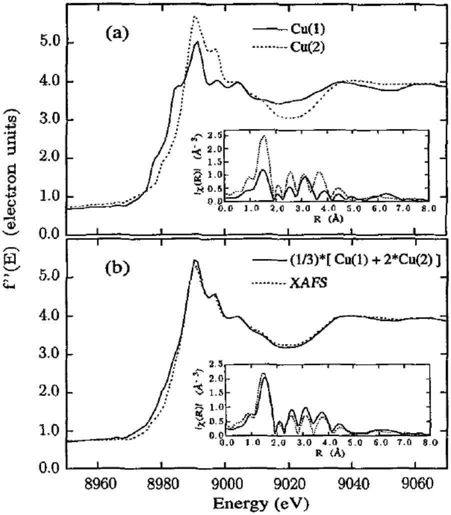

The two Cu sites are distinctly different in both edge position and shape

the Fourier transform is also significantly different for the two sites, particularly the amplitude of the Cu-O peak in the real-space EXAFS

combined in the 2:1 ratio, the measured EXAFS is recovered

'Separated anomalous scattering amplitudes for the inequivalent Cu sites in $YBa_2Cu_3O_{7-\delta}$ using DAFS," J.O. Cross, M. Newville, L.B. Sorensen, H.J. Straiger, C.E. Bouldin, and J.C. Woicik, *J. Phys.* **C2**, 745-747 (1997).

DAFS of $YBa_2Cu_3O_7$

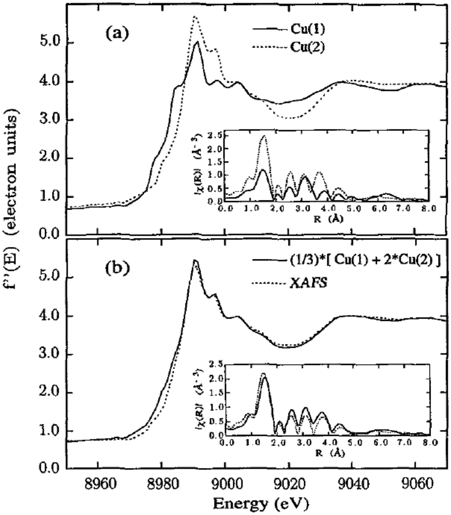

The two Cu sites are distinctly different in both edge position and shape

the Fourier transform is also significantly different for the two sites, particularly the amplitude of the Cu-O peak in the real-space EXAFS

combined in the 2:1 ratio, the measured EXAFS is recovered

This data was taken on a single crystal but it is also possible to measure powders using DAFS

'Separated anomalous scattering amplitudes for the inequivalent Cu sites in $YBa_2Cu_3O_{7-\delta}$ using DAFS," J.O. Cross, M. Newville, L.B. Sorensen, H.J. Straiger, C.E. Bouldin, and J.C. Woicik, *J. Phys.* **C2**, 745-747 (1997).

DAFS of maghemite γ-Fe_2O_3 shells

Nanoparticles of ferromagnetic Fe metal surrounded by a weakly magnetic γ-Fe_2O_3 (maghemite) have potential applications for high density recording media

"Diffraction anomalous fine structure study of iron/iron oxide nanoparticles," C. Meneghini, F. Boscherini, L. Pasquini, and H. Renevier, *J. Appl. Cryst.* **42**, 642-645 (2009)

DAFS of maghemite γ-Fe_2O_3 shells

Nanoparticles of ferromagnetic Fe metal surrounded by a weakly magnetic γ-Fe_2O_3 (maghemite) have potential applications for high density recording media

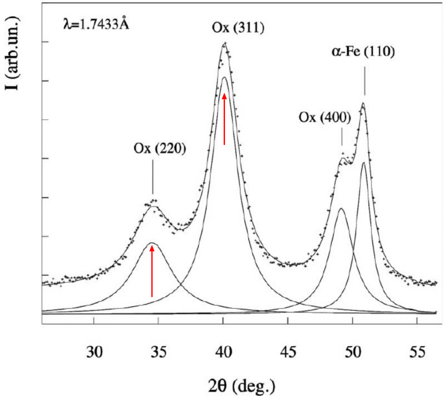

"Diffraction anomalous fine structure study of iron/iron oxide nanoparticles," C. Meneghini, F. Boscherini, L. Pasquini, and H. Renevier, *J. Appl. Cryst.* **42**, 642-645 (2009)

DAFS of maghemite γ-Fe_2O_3 shells

Nanoparticles of ferromagnetic Fe metal surrounded by a weakly magnetic γ-Fe_2O_3 (maghemite) have potential applications for high density recording media

Because of the presence of Fe in both the core and the shell it is not possible to use EXAFS to study the local structure of the oxide shell directly

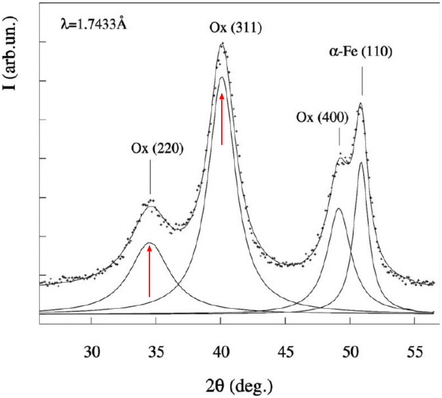

"Diffraction anomalous fine structure study of iron/iron oxide nanoparticles," C. Meneghini, F. Boscherini, L. Pasquini, and H. Renevier, *J. Appl. Cryst.* **42**, 642-645 (2009)

DAFS of maghemite γ-Fe_2O_3 shells

Nanoparticles of ferromagnetic Fe metal surrounded by a weakly magnetic γ-Fe_2O_3 (maghemite) have potential applications for high density recording media

Because of the presence of Fe in both the core and the shell it is not possible to use EXAFS to study the local structure of the oxide shell directly

DAFS on the powder samples has the potential to focus solely on the γ-Fe_2O_3 to the exclusion of the metallic core by measuring the oscillations in the oxide (220) and (311) reflections

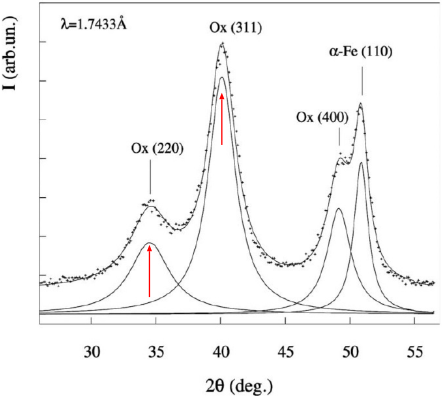

"Diffraction anomalous fine structure study of iron/iron oxide nanoparticles," C. Meneghini, F. Boscherini, L. Pasquini, and H. Renevier, *J. Appl. Cryst.* **42**, 642-645 (2009)

DAFS of maghemite γ-Fe_2O_3 shells

With DAFS, not only was the interference from the metal cores avoided but it was possible to separate the two distinct sites in the maghemite (γ-Fe_2O_3) structure

"Diffraction anomalous fine structure study of iron/iron oxide nanoparticles," C. Meneghini, F. Boscherini, L. Pasquini, and H. Renevier, *J. Appl. Cryst.* **42**, 642-645 (2009)

DAFS of maghemite γ-Fe_2O_3 shells

With DAFS, not only was the interference from the metal cores avoided but it was possible to separate the two distinct sites in the maghemite (γ-Fe_2O_3) structure

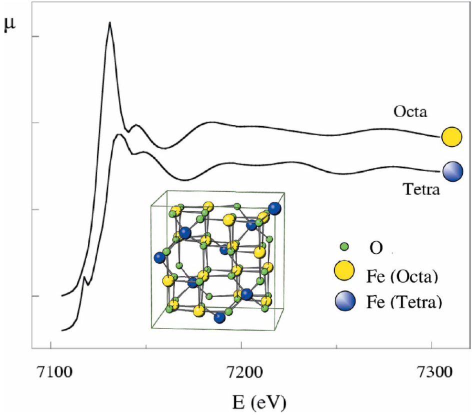

"Diffraction anomalous fine structure study of iron/iron oxide nanoparticles," C. Meneghini, F. Boscherini, L. Pasquini, and H. Renevier, *J. Appl. Cryst.* **42**, 642-645 (2009)

DAFS of maghemite γ-Fe_2O_3 shells

With DAFS, not only was the interference from the metal cores avoided but it was possible to separate the two distinct sites in the maghemite (γ-Fe_2O_3) structure

The simulation shows how the tetrahedral Fe site which contributes to the (220) peak and the octahedral site which contributes to the (311) peak differ subtly in the EXAFS region

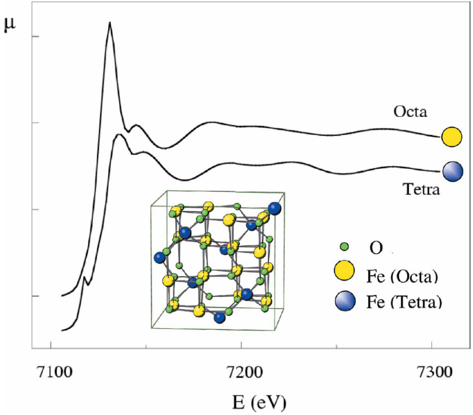

"Diffraction anomalous fine structure study of iron/iron oxide nanoparticles," C. Meneghini, F. Boscherini, L. Pasquini, and H. Renevier, *J. Appl. Cryst.* **42**, 642-645 (2009)

DAFS of maghemite γ-Fe_2O_3 shells

With DAFS, not only was the interference from the metal cores avoided but it was possible to separate the two distinct sites in the maghemite (γ-Fe_2O_3) structure

The simulation shows how the tetrahedral Fe site which contributes to the (220) peak and the octahedral site which contributes to the (311) peak differ subtly in the EXAFS region

The EXAFS fits of the two sites correspond closely to the nominal structure of maghemite with some observed oxygen vacancies

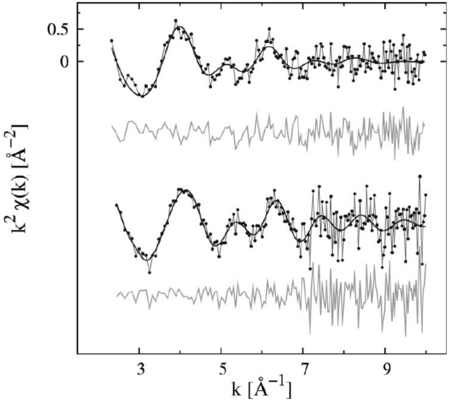

"Diffraction anomalous fine structure study of iron/iron oxide nanoparticles," C. Meneghini, F. Boscherini, L. Pasquini, and H. Renevier, *J. Appl. Cryst.* **42**, 642-645 (2009)

X-ray Raman (XRR)

X-ray Raman is a way to measure the XAS spectrum of light elements whose absorption edges are below 2 keV.

X-ray Raman (XRR)

X-ray Raman is a way to measure the XAS spectrum of light elements whose absorption edges are below 2 keV.

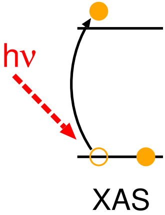

The x-ray absorption event consists of the absorption of a photon and production of a photoelectron

X-ray Raman (XRR)

X-ray Raman is a way to measure the XAS spectrum of light elements whose absorption edges are below 2 keV.

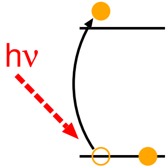

XAS

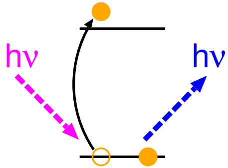

XRR

The x-ray absorption event consists of the absorption of a photon and production of a photoelectron

X-ray Raman is a similar process which produces a photoelectron but is an inelastic scattering process with an outgoing photon of lower energy

X-ray Raman (XRR)

X-ray Raman is a way to measure the XAS spectrum of light elements whose absorption edges are below 2 keV.

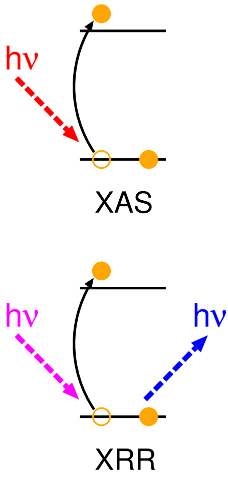

The x-ray absorption event consists of the absorption of a photon and production of a photoelectron

X-ray Raman is a similar process which produces a photoelectron but is an inelastic scattering process with an outgoing photon of lower energy

The incoming x-rays are high energy and the detector is set to measure outgoing x-rays which are at a fixed energy.

X-ray Raman (XRR)

X-ray Raman is a way to measure the XAS spectrum of light elements whose absorption edges are below 2 keV.

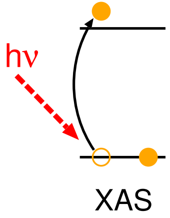

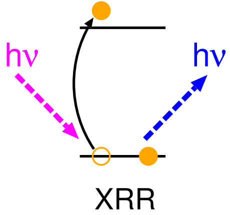

The x-ray absorption event consists of the absorption of a photon and production of a photoelectron

X-ray Raman is a similar process which produces a photoelectron but is an inelastic scattering process with an outgoing photon of lower energy

The incoming x-rays are high energy and the detector is set to measure outgoing x-rays which are at a fixed energy. The incoming energy is scanned and the processes detected depend on the difference in energy

The XRR experiment

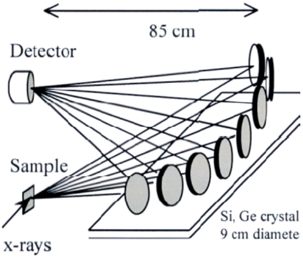

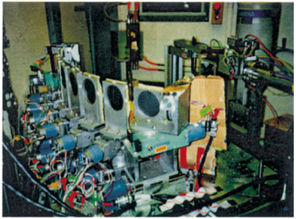

"Bulk-sensitive XAS characterization of light elements: from x-ray Raman scattering to x-ray Raman spectroscopy," U. Bergmann, P. Glatzel, and S. Cramer, *Microchem. J.* **71**, 221-230 (2002)

The XRR experiment

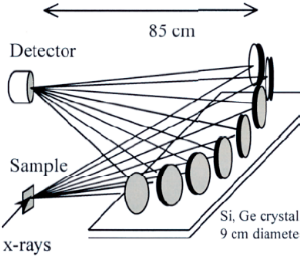

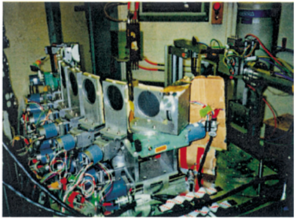

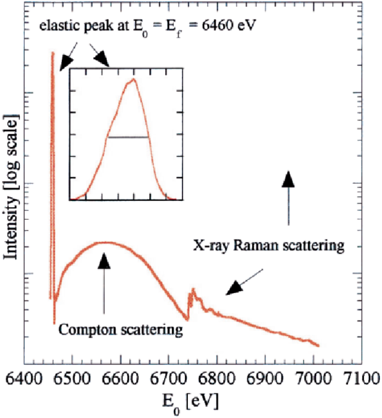

"Bulk-sensitive XAS characterization of light elements: from x-ray Raman scattering to x-ray Raman spectroscopy," U. Bergmann, P. Glatzel, and S. Cramer, *Microchem. J.* **71**, 221-230 (2002)

XRR spectra of light elements

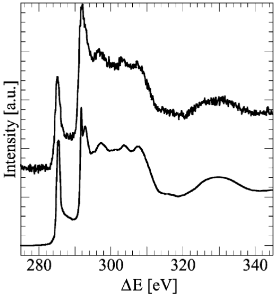

Comparison of XRR and XAS on graphite

"Bulk-sensitive XAS characterization of light elements: from x-ray Raman scattering to x-ray Raman spectroscopy," U. Bergmann, P. Glatzel, and S. Cramer, *Microchem. J.* **71**, 221-230 (2002)

XRR spectra of light elements

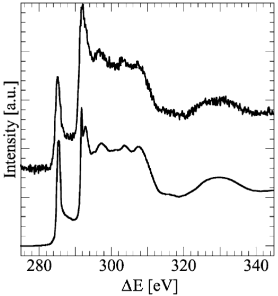

Comparison of XRR and XAS on graphite

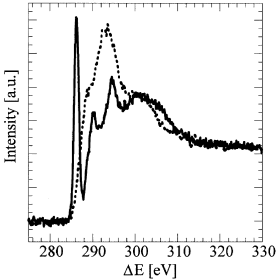

Aromatic (solid) and aliphatic (dashed) carbon K-edge x-ray Raman spectra

"Bulk-sensitive XAS characterization of light elements: from x-ray Raman scattering to x-ray Raman spectroscopy," U. Bergmann, P. Glatzel, and S. Cramer, *Microchem. J.* **71**, 221-230 (2002)

XRR spectra of light elements

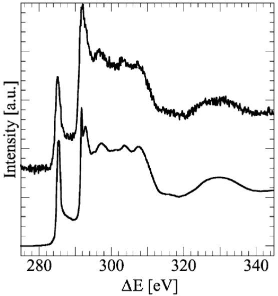

Comparison of XRR and XAS on graphite

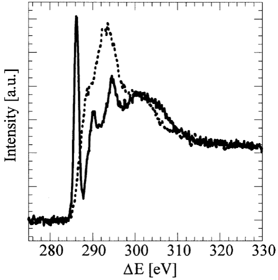

Aromatic (solid) and aliphatic (dashed) carbon K-edge x-ray Raman spectra

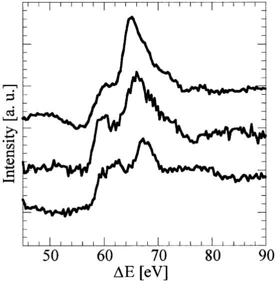

Li K-edge spectra for $LiOH \cdot H_2O$ (top), Li_2CO_3 (middle), and Li_4SiO_4 (bottom).

"Bulk-sensitive XAS characterization of light elements: from x-ray Raman scattering to x-ray Raman spectroscopy," U. Bergmann, P. Glatzel, and S. Cramer, *Microchem. J.* **71**, 221-230 (2002)

X-ray emission spectroscopy (XES)

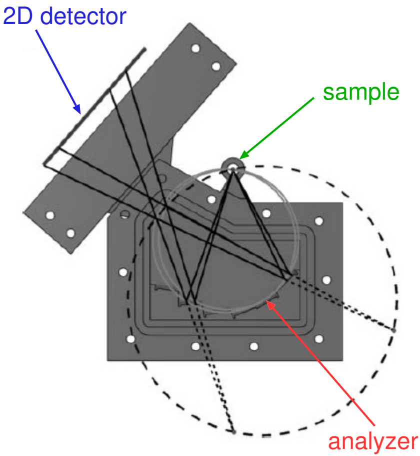

X-ray emission spectroscopy (XES)

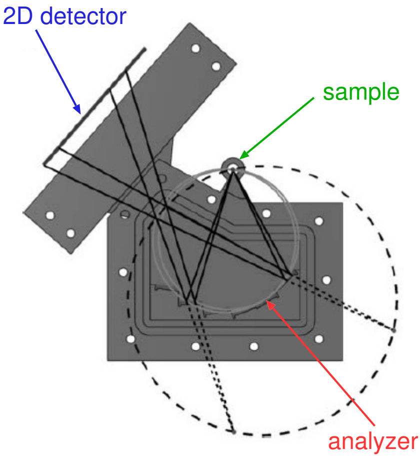

Normally a fluorescence line is measured with a detector which cannot resolve its fine structure

X-ray emission spectroscopy (XES)

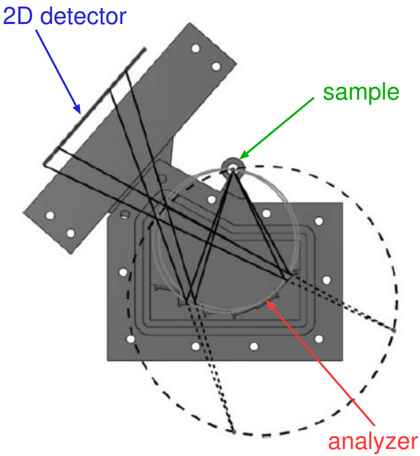

Normally a fluorescence line is measured with a detector which cannot resolve its fine structure

with an XES analyzer, the fine features of the emission spectrum are separated

X-ray emission spectroscopy (XES)

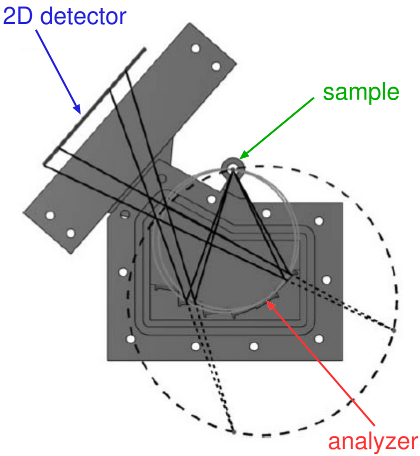

Normally a fluorescence line is measured with a detector which cannot resolve its fine structure

with an XES analyzer, the fine features of the emission spectrum are separated

the analyzer crystal diffracts different energies at different angles, spreading the different energies over the face of the 2D detector

X-ray emission spectroscopy (XES)

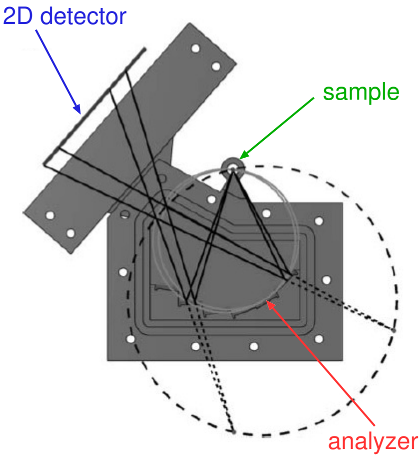

Normally a fluorescence line is measured with a detector which cannot resolve its fine structure

with an XES analyzer, the fine features of the emission spectrum are separated

the analyzer crystal diffracts different energies at different angles, spreading the different energies over the face of the 2D detector

each crystal in the analyzer collects the same range of fluorescence energies for a larger solid angle

X-ray emission spectroscopy (XES)

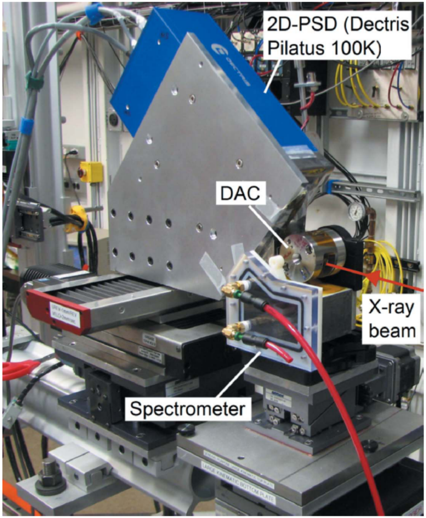

Normally a fluorescence line is measured with a detector which cannot resolve its fine structure

with an XES analyzer, the fine features of the emission spectrum are separated

the analyzer crystal diffracts different energies at different angles, spreading the different energies over the face of the 2D detector

each crystal in the analyzer collects the same range of fluorescence energies for a larger solid angle

XES spectrometer performance

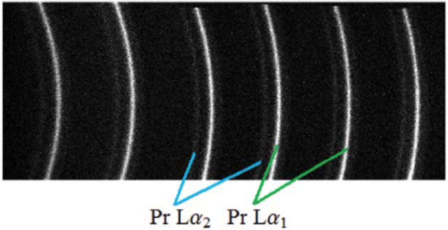

XES spectrometer performance

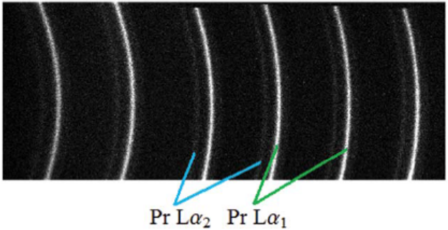

The Pr-containing sample is placed in a diamond anvil high pressure cell (DAC) and illuminated with energies near the Pr L_3 edge (5964 eV)

XES spectrometer performance

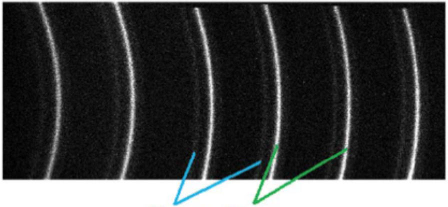

The Pr-containing sample is placed in a diamond anvil high pressure cell (DAC) and illuminated with energies near the Pr L_3 edge (5964 eV)

the spectrometer clearly separates the Pr Lα_1 (5035.2 eV) and Lα_2 (5015.7 eV) emission lines

XES spectrometer performance

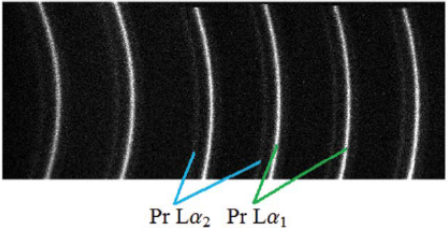

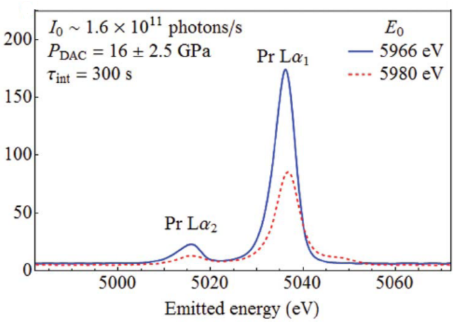

The Pr-containing sample is placed in a diamond anvil high pressure cell (DAC) and illuminated with energies near the Pr L_3 edge (5964 eV)

the spectrometer clearly separates the Pr $L\alpha_1$ (5035.2 eV) and $L\alpha_2$ (5015.7 eV) emission lines

after integration, the two peaks can be seen to change relative intensities and even position as a function of the incident energy: just at the absorption edge and 14 eV higher

Resonant inelastic x-ray scattering (RIXS)

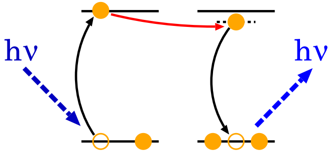

RIXS probes electronic states near the absorption edge

"Resonant inelastic x-ray scattering," P.M. Platzman and E.D. Isaacs, *Phys. Rev. B* **57**, 11108 (1998)

Resonant inelastic x-ray scattering (RIXS)

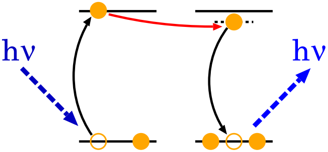

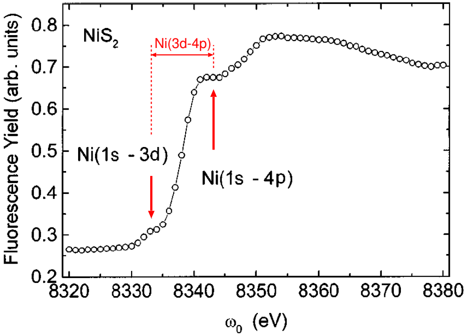

RIXS probes electronic states near the absorption edge

The presence of a strong absorption increases the cross section of the inelastic process which probes electronic excitations otherwise challenging to measure

"Resonant inelastic x-ray scattering," P.M. Platzman and E.D. Isaacs, *Phys. Rev. B* **57**, 11108 (1998)

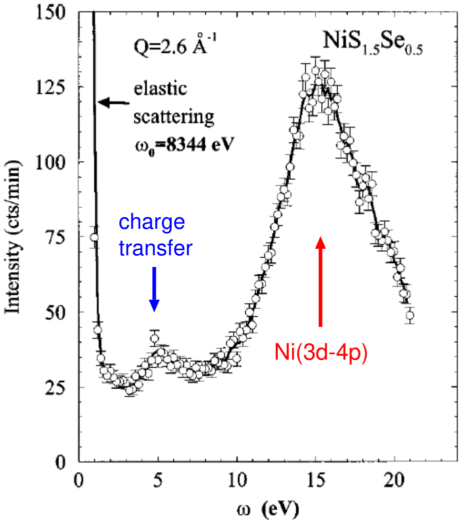

RIXS probes electronic states near the absorption edge

The presence of a strong absorption increases the cross section of the inelastic process which probes electronic excitations otherwise challenging to measure

"Resonant inelastic x-ray scattering," P.M. Platzman and E.D. Isaacs, *Phys. Rev. B* **57**, 11108 (1998)

Resonant inelastic x-ray scattering (RIXS)

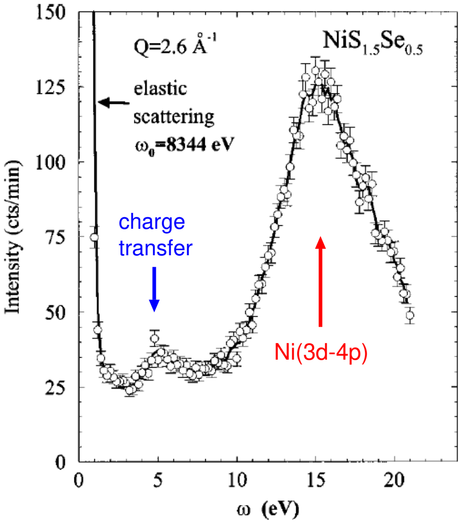

RIXS probes electronic states near the absorption edge

The presence of a strong absorption increases the cross section of the inelastic process which probes electronic excitations otherwise challenging to measure

The RIXS technique can also be used to study a wide variety of electronic excitations as a function of momentum transfer

"Resonant inelastic x-ray scattering," P.M. Platzman and E.D. Isaacs, *Phys. Rev. B* **57**, 11108 (1998)

Spin-orbit Mott state in Sr_2IrO_4

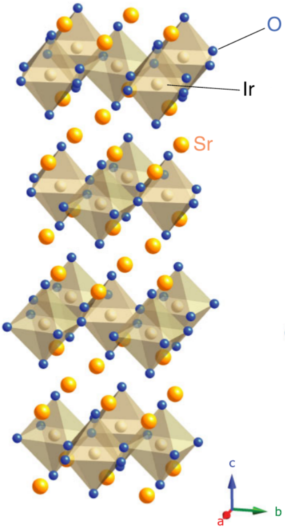

Sr_2IrO_4 is a structural analog to the high T_C superconductor $La_(2-x)Sr_xCuO_4$ and to the Fermi liquid metal Sr_2RhO_4

"Novel $J_{eff} = 1/2$ Mott state induced by relativistic spin-orbit coupling in Sr_2IrO_4," B.J. Kim, H. Jin, S.J. Moon, J.-Y. Kim, B.-G. Park, C.S. Leem, J. Yu, T.W. Noh, C. Kim, S.-J. Oh, J.-H. Park, V. Durairaj, G. Cao, and E. Rotenberg, *Phys. Rev. Lett.* **101**, 076402 (2008).

Spin-orbit Mott state in Sr_2IrO_4

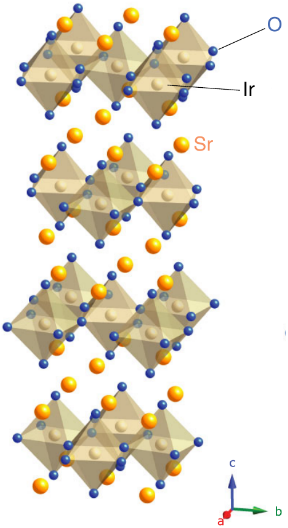

Sr_2IrO_4 is a structural analog to the high T_C superconductor $La_(2-x)Sr_xCuO_4$ and to the Fermi liquid metal Sr_2RhO_4

The $(5d^5)$ configuration suggests that this material is a metal with a half-filled band, however, Sr_2IrO_4 is an antiferromagnetism insulator

"Novel $J_{eff} = 1/2$ Mott state induced by relativistic spin-orbit coupling in Sr_2IrO_4," B.J. Kim, H. Jin, S.J. Moon, J.-Y. Kim, B.-G. Park, C.S. Leem, J. Yu, T.W. Noh, C. Kim, S.-J. Oh, J.-H. Park, V. Durairaj, G. Cao, and E. Rotenberg, *Phys. Rev. Lett.* **101**, 076402 (2008).

Spin-orbit Mott state in Sr_2IrO_4

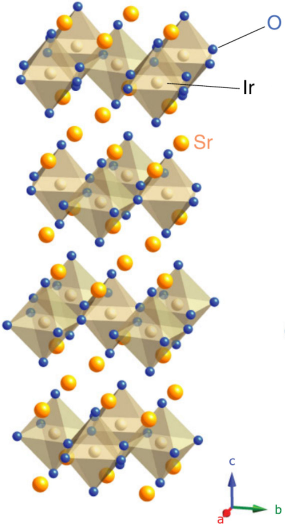

Sr_2IrO_4 is a structural analog to the high T_C superconductor $La_(2-x)Sr_xCuO_4$ and to the Fermi liquid metal Sr_2RhO_4

The $(5d^5)$ configuration suggests that this material is a metal with a half-filled band, however, Sr_2IrO_4 is an antiferromagnetism insulator

This behavior is likely due to the stronger spin-orbit coupling found in 5d states compared to 3d and 4d systems

"Novel $J_{eff} = 1/2$ Mott state induced by relativistic spin-orbit coupling in Sr_2IrO_4," B.J. Kim, H. Jin, S.J. Moon, J.-Y. Kim, B.-G. Park, C.S. Leem, J. Yu, T.W. Noh, C. Kim, S.-J. Oh, J.-H. Park, V. Durairaj, G. Cao, and E. Rotenberg, *Phys. Rev. Lett.* **101**, 076402 (2008).

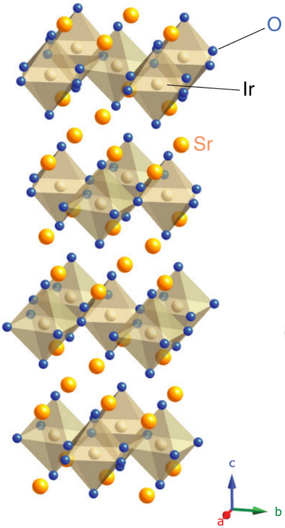

- Sr_2IrO_4 is a structural analog to the high T_C superconductor $La_(2-x)Sr_xCuO_4$ and to the Fermi liquid metal Sr_2RhO_4
- The ($5d^5$) configuration suggests that this material is a metal with a half-filled band, however, Sr_2IrO_4 is an antiferromagnetism insulator
- This behavior is likely due to the stronger spin-orbit coupling found in $5d$ states compared to $3d$ and $4d$ systems
- Starting in 2008, a group from South Korea grew a single crystal of Sr_2IrO_4 and published a series of papers that studied its electronic states using resonant x-ray techniques among others

"Novel $J_{eff} = 1/2$ Mott state induced by relativistic spin-orbit coupling in Sr_2IrO_4," B.J. Kim, H. Jin, S.J. Moon, J.-Y. Kim, B.-G. Park, C.S. Leem, J. Yu, T.W. Noh, C. Kim, S.-J. Oh, J.-H. Park, V. Durairaj, G. Cao, and E. Rotenberg, *Phys. Rev. Lett.* **101**, 076402 (2008).

Spin-orbit Mott state in Sr_2IrO_4

The electronic properties of Sr_2IrO_4 arise from a spin-orbit coupling that is much larger than the Hubbard model Coulomb self-energy, U

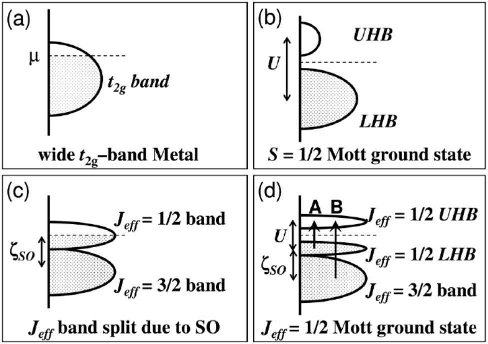

"Novel $J_{eff} = 1/2$ Mott state induced by relativistic spin-orbit coupling in Sr_2IrO_4," B.J. Kim, H. Jin, S.J. Moon, J.-Y. Kim, B.-G. Park, C.S. Leem, J. Yu, T.W. Noh, C. Kim, S.-J. Oh, J.-H. Park, V. Durairaj, G. Cao, and E. Rotenberg, *Phys. Rev. Lett.* **101**, 076402 (2008).

Spin-orbit Mott state in Sr_2IrO_4

The electronic properties of Sr_2IrO_4 arise from a spin-orbit coupling that is much larger than the Hubbard model Coulomb self-energy, U

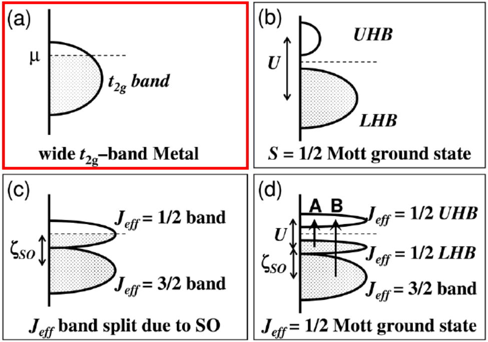

(a) the unperturbed t_{2g} triplet has one empty state

"Novel $J_{eff} = 1/2$ Mott state induced by relativistic spin-orbit coupling in Sr_2IrO_4," B.J. Kim, H. Jin, S.J. Moon, J.-Y. Kim, B.-G. Park, C.S. Leem, J. Yu, T.W. Noh, C. Kim, S.-J. Oh, J.-H. Park, V. Durairaj, G. Cao, and E. Rotenberg, *Phys. Rev. Lett.* **101**, 076402 (2008).

Spin-orbit Mott state in Sr_2IrO_4

The electronic properties of Sr_2IrO_4 arise from a spin-orbit coupling that is much larger than the Hubbard model Coulomb self-energy, U

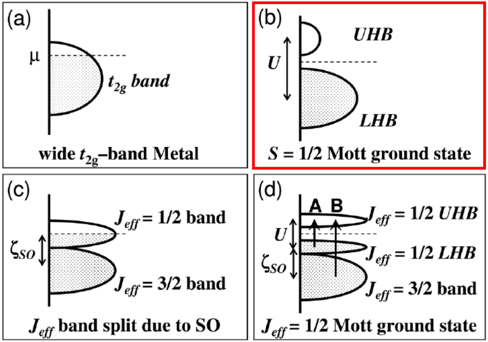

(a) the unperturbed t_{2g} triplet has one empty state

(b) with a large U, the system becomes an insulator, like La_2CuO_4

"Novel $J_{eff} = 1/2$ Mott state induced by relativistic spin-orbit coupling in Sr_2IrO_4," B.J. Kim, H. Jin, S.J. Moon, J.-Y. Kim, B.-G. Park, C.S. Leem, J. Yu, T.W. Noh, C. Kim, S.-J. Oh, J.-H. Park, V. Durairaj, G. Cao, and E. Rotenberg, *Phys. Rev. Lett.* **101**, 076402 (2008).

Spin-orbit Mott state in Sr_2IrO_4

The electronic properties of Sr_2IrO_4 arise from a spin-orbit coupling that is much larger than the Hubbard model Coulomb self-energy, U

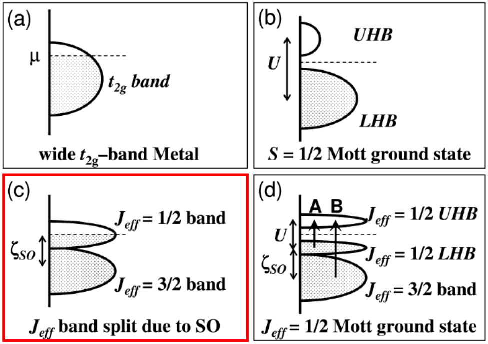

(a) the unperturbed t_{2g} triplet has one empty state

(b) with a large U, the system becomes an insulator, like La_2CuO_4

(c) if the spin-orbit coupling is large the $J_{eff} = \frac{1}{2}$ doublet splits above the $J_{eff} = \frac{3}{2}$ states and the system remains a metal

"Novel $J_{eff} = 1/2$ Mott state induced by relativistic spin-orbit coupling in Sr_2IrO_4," B.J. Kim, H. Jin, S.J. Moon, J.-Y. Kim, B.-G. Park, C.S. Leem, J. Yu, T.W. Noh, C. Kim, S.-J. Oh, J.-H. Park, V. Durairaj, G. Cao, and E. Rotenberg, *Phys. Rev. Lett.* **101**, 076402 (2008).

Spin-orbit Mott state in Sr_2IrO_4

The electronic properties of Sr_2IrO_4 arise from a spin-orbit coupling that is much larger than the Hubbard model Coulomb self-energy, U

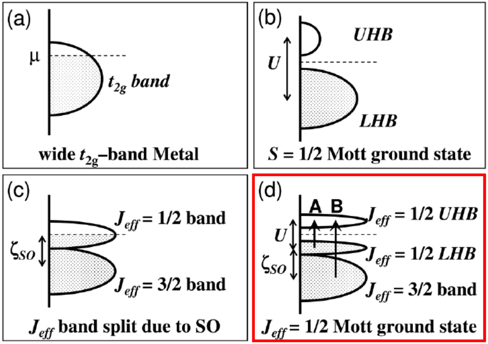

"Novel $J_{eff} = 1/2$ Mott state induced by relativistic spin-orbit coupling in Sr_2IrO_4," B.J. Kim, H. Jin, S.J. Moon, J.-Y. Kim, B.-G. Park, C.S. Leem, J. Yu, T.W. Noh, C. Kim, S.-J. Oh, J.-H. Park, V. Durairaj, G. Cao, and E. Rotenberg, *Phys. Rev. Lett.* **101**, 076402 (2008).

(a) the unperturbed t_{2g} triplet has one empty state

(b) with a large U, the system becomes an insulator, like La_2CuO_4

(c) if the spin-orbit coupling is large the $J_{eff} = \frac{1}{2}$ doublet splits above the $J_{eff} = \frac{3}{2}$ states and the system remains a metal

(d) the Hubbard U splits the $J_{eff} = \frac{1}{2}$ into an upper and lower band, creating an insulator

Resonant x-ray scattering on Sr_2IrO_4

Below 240K, Sr_2IrO_4 orders antiferrromagnetically and with a modest applied field ($H > 0.3$ T), becomes weakly ferromagnetic

"Phase-sensitive observation of a spin-orbital Mott state in Sr_2IrO_4," B.J. Kim, H. Osumi, T. Komesu, S. Sakai, T. Morita, H. Tagaki, and T. Arima, *Science* **323**, 1329-1332 (2009).

Resonant x-ray scattering on Sr_2IrO_4

Below 240K, Sr_2IrO_4 orders antiferrromagnetically and with a modest applied field ($H > 0.3$ T), becomes weakly ferromagnetic

Using resonant x-ray scattering, at the L_3 edge of iridium, it is possible to excite the empty upper Hubbard $J_{eff} = \frac{1}{2}$ band and enchance the magnetic x-ray scattering

"Phase-sensitive observation of a spin-orbital Mott state in Sr_2IrO_4," B.J. Kim, H. Osumi, T. Komesu, S. Sakai, T. Morita, H. Tagaki, and T. Arima, *Science* **323**, 1329-1332 (2009).

Resonant x-ray scattering on Sr_2IrO_4

Below 240K, Sr_2IrO_4 orders antiferrromagnetically and with a modest applied field ($H > 0.3$ T), becomes weakly ferromagnetic

Using resonant x-ray scattering, at the L_3 edge of iridium, it is possible to excite the empty upper Hubbard $J_{eff} = \frac{1}{2}$ band and enchance the magnetic x-ray scattering

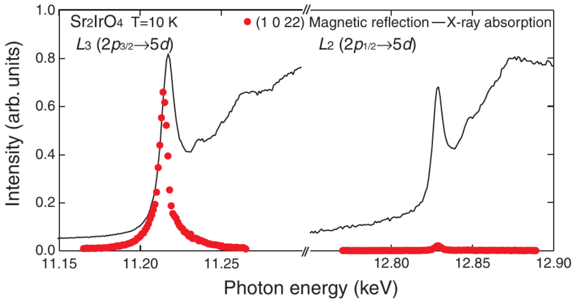

The (1 0 22) magnetic reflection (red circles) is enhanced at the L_3 edge but not at the L_2 edge due to interference effects

"Phase-sensitive observation of a spin-orbital Mott state in Sr_2IrO_4," B.J. Kim, H. Osumi, T. Komesu, S. Sakai, T. Morita, H. Tagaki, and T. Arima, *Science* **323**, 1329-1332 (2009).

Resonant x-ray scattering on Sr_2IrO_4

Below 240K, Sr_2IrO_4 orders antiferrromagnetically and with a modest applied field ($H > 0.3$ T), becomes weakly ferromagnetic

Using resonant x-ray scattering, at the L_3 edge of iridium, it is possible to excite the empty upper Hubbard $J_{eff} = \frac{1}{2}$ band and enchance the magnetic x-ray scattering

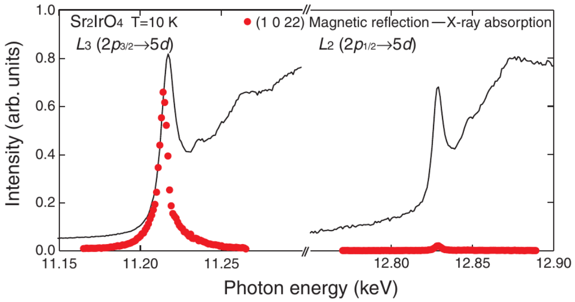

The (1 0 22) magnetic reflection (red circles) is enhanced at the L_3 edge but not at the L_2 edge due to interference effects

This enhancement by a factor of 100× permits a detailed study of the magnetic structure

"Phase-sensitive observation of a spin-orbital Mott state in Sr_2IrO_4," B.J. Kim, H. Osumi, T. Komesu, S. Sakai, T. Morita, H. Tagaki, and T. Arima, *Science* **323**, 1329-1332 (2009).

Probing Sr_2IrO_4 electronic states by RIXS

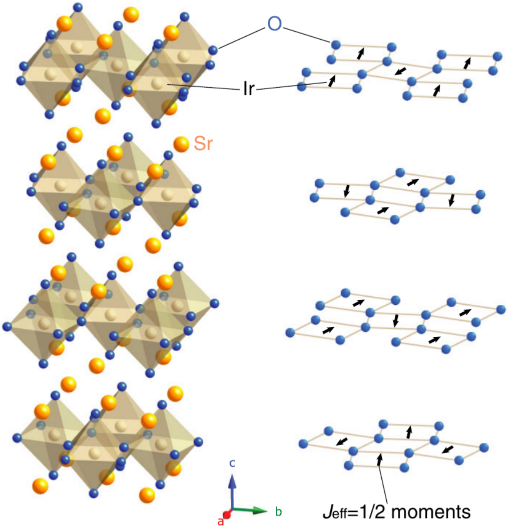

The insulating antiferromagnetic state of Sr_2IrO_4 has canted magnetic moments oriented in the Ir-O planes

"Magnetic excitation spectra of Sr_2IrO_4 probed by resonant inelastic x-ray scattering: Establishing links to cuprate superconductors," J. Kim, D. Casa, M.H. Upton, T. Gog, Y.-J. Kim, J.F. Mitchell, M. van Veenendaal, M. Daghofer, J. van den Brink, G. Khaliullin, and B.J. Kim, *Phys. Rev. Lett.* **108**, 177003 (2012).

Probing Sr_2IrO_4 electronic states by RIXS

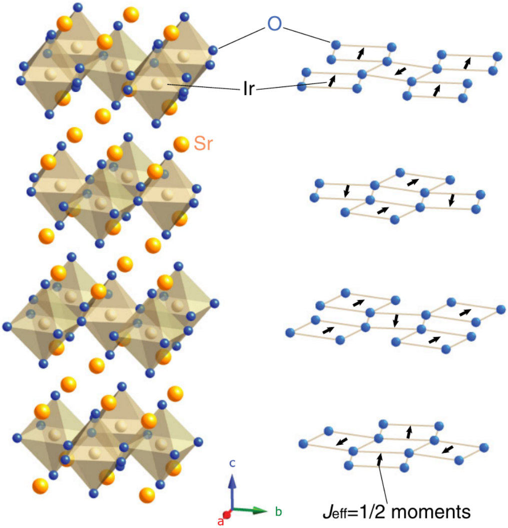

The insulating antiferromagnetic state of Sr_2IrO_4 has canted magnetic moments oriented in the Ir-O planes

This spin lattice has magnetic excitations which can be probed using resonant inelastic x-ray scattering since there are empty states $J_{eff} = \frac{1}{2}$ just above the Fermi level

"Magnetic excitation spectra of Sr_2IrO_4 probed by resonant inelastic x-ray scattering: Establishing links to cuprate superconductors," J. Kim, D. Casa, M.H. Upton, T. Gog, Y.-J. Kim, J.F. Mitchell, M. van Veenendaal, M. Daghofer, J. van den Brink, G. Khaliullin, and B.J. Kim, *Phys. Rev. Lett.* **108**, 177003 (2012).

Probing Sr_2IrO_4 electronic states by RIXS

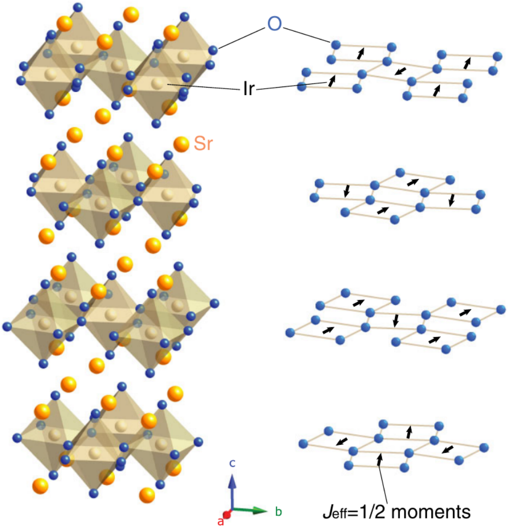

The insulating antiferromagnetic state of Sr_2IrO_4 has canted magnetic moments oriented in the Ir-O planes

This spin lattice has magnetic excitations which can be probed using resonant inelastic x-ray scattering since there are empty states $J_{eff} = \frac{1}{2}$ just above the Fermi level

Energy loss spectra were measured as a function of q at the Ir L_3 edge

"Magnetic excitation spectra of Sr_2IrO_4 probed by resonant inelastic x-ray scattering: Establishing links to cuprate superconductors," J. Kim, D. Casa, M.H. Upton, T. Gog, Y.-J. Kim, J.F. Mitchell, M. van Veenendaal, M. Daghofer, J. van den Brink, G. Khaliullin, and B.J. Kim, *Phys. Rev. Lett.* **108**, 177003 (2012).

Probing Sr_2IrO_4 electronic states by RIXS

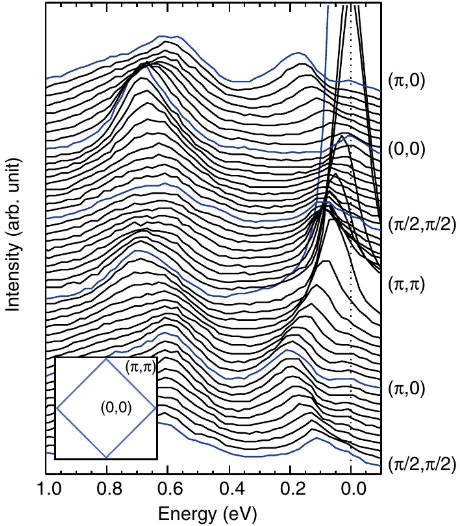

The Bragg peak is clear at energy loss of zero in the (π,π) direction

"Magnetic excitation spectra of Sr_2IrO_4 probed by resonant inelastic x-ray scattering: Establishing links to cuprate superconductors," J. Kim, D. Casa, M.H. Upton, T. Gog, Y.-J. Kim, J.F. Mitchell, M. van Veenendaal, M. Daghofer, J. van den Brink, G. Khaliullin, and B.J. Kim, *Phys. Rev. Lett.* **108**, 177003 (2012).

Probing Sr_2IrO_4 electronic states by RIXS

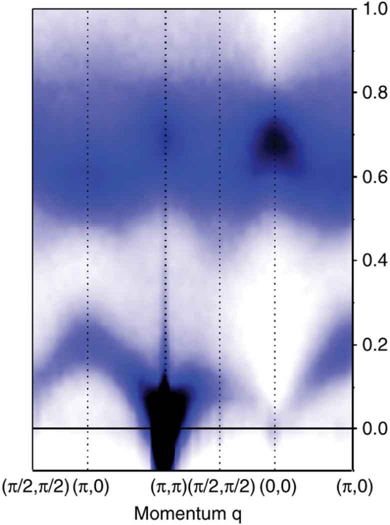

The Bragg peak is clear at energy loss of zero in the (π,π) direction

When lines of constant energy loss are taken through the individual scans and combined to give a contour plot of the excitations the different bands and their shapes as a function of momentum are visible

"Magnetic excitation spectra of Sr_2IrO_4 probed by resonant inelastic x-ray scattering: Establishing links to cuprate superconductors," J. Kim, D. Casa, M.H. Upton, T. Gog, Y.-J. Kim, J.F. Mitchell, M. van Veenendaal, M. Daghofer, J. van den Brink, G. Khaliullin, and B.J. Kim, *Phys. Rev. Lett.* **108**, 177003 (2012).

Probing Sr_2IrO_4 electronic states by RIXS

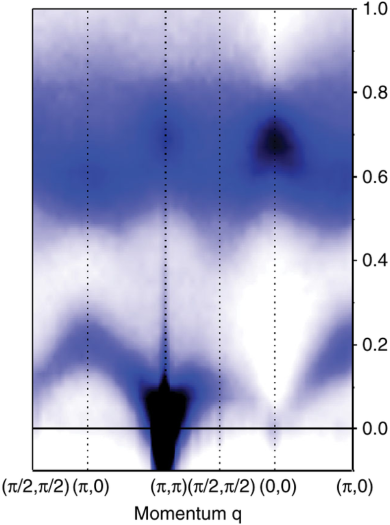

The Bragg peak is clear at energy loss of zero in the (π,π) direction

When lines of constant energy loss are taken through the individual scans and combined to give a contour plot of the excitations the different bands and their shapes as a function of momentum are visible

Taking the second derivative enhances the band structure further

"Magnetic excitation spectra of Sr_2IrO_4 probed by resonant inelastic x-ray scattering: Establishing links to cuprate superconductors," J. Kim, D. Casa, M.H. Upton, T. Gog, Y.-J. Kim, J.F. Mitchell, M. van Veenendaal, M. Daghofer, J. van den Brink, G. Khaliullin, and B.J. Kim, *Phys. Rev. Lett.* **108**, 177003 (2012).

Probing Sr_2IrO_4 electronic states by RIXS

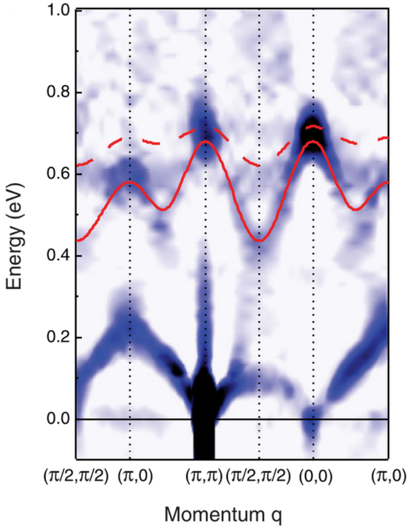

"Magnetic excitation spectra of Sr_2IrO_4 probed by resonant inelastic x-ray scattering: Establishing links to cuprate superconductors," J. Kim, D. Casa, M.H. Upton, T. Gog, Y.-J. Kim, J.F. Mitchell, M. van Veenendaal, M. Daghofer, J. van den Brink, G. Khaliullin, and B.J. Kim, *Phys. Rev. Lett.* **108**, 177003 (2012).

Probing Sr_2IrO_4 electronic states by RIXS

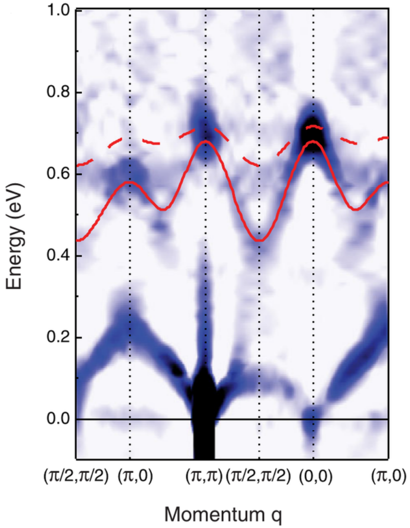

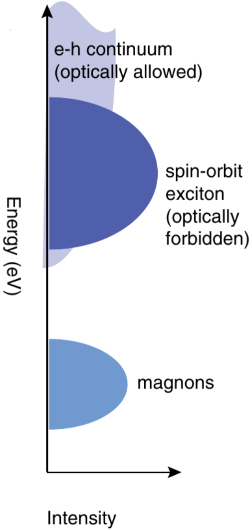

"Magnetic excitation spectra of Sr_2IrO_4 probed by resonant inelastic x-ray scattering: Establishing links to cuprate superconductors," J. Kim, D. Casa, M.H. Upton, T. Gog, Y.-J. Kim, J.F. Mitchell, M. van Veenendaal, M. Daghofer, J. van den Brink, G. Khaliullin, and B.J. Kim, *Phys. Rev. Lett.* **108**, 177003 (2012).

Probing Sr_2IrO_4 electronic states by RIXS

The RIXS measurements along with theoretical calculations clarify the electronic processes occurring in Sr_2IrO_4

"Magnetic excitation spectra of Sr_2IrO_4 probed by resonant inelastic x-ray scattering: Establishing links to cuprate superconductors," J. Kim, D. Casa, M.H. Upton, T. Gog, Y.-J. Kim, J.F. Mitchell, M. van Veenendaal, M. Daghofer, J. van den Brink, G. Khaliullin, and B.J. Kim, *Phys. Rev. Lett.* **108**, 177003 (2012).

Probing Sr_2IrO_4 electronic states by RIXS

The RIXS measurements along with theoretical calculations clarify the electronic processes occurring in Sr_2IrO_4

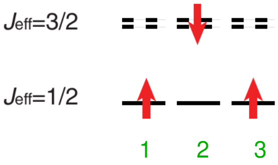

left – a exciton created by RIXS leaves a hole the $J_{eff} = \frac{3}{2}$ state on site 2

"Magnetic excitation spectra of Sr_2IrO_4 probed by resonant inelastic x-ray scattering: Establishing links to cuprate superconductors," J. Kim, D. Casa, M.H. Upton, T. Gog, Y.-J. Kim, J.F. Mitchell, M. van Veenendaal, M. Daghofer, J. van den Brink, G. Khaliullin, and B.J. Kim, *Phys. Rev. Lett.* **108**, 177003 (2012).

Probing Sr_2IrO_4 electronic states by RIXS

The RIXS measurements along with theoretical calculations clarify the electronic processes occurring in Sr_2IrO_4

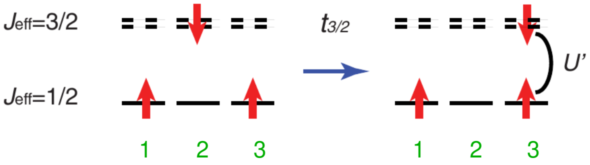

left – a exciton created by RIXS leaves a hole the $J_{eff} = \frac{3}{2}$ state on site 2

center – the hole in the $J_{eff} = \frac{3}{2}$ state hops to site 3

"Magnetic excitation spectra of Sr_2IrO_4 probed by resonant inelastic x-ray scattering: Establishing links to cuprate superconductors," J. Kim, D. Casa, M.H. Upton, T. Gog, Y.-J. Kim, J.F. Mitchell, M. van Veenendaal, M. Daghofer, J. van den Brink, G. Khaliullin, and B.J. Kim, *Phys. Rev. Lett.* **108**, 177003 (2012).

Probing Sr_2IrO_4 electronic states by RIXS

The RIXS measurements along with theoretical calculations clarify the electronic processes occurring in Sr_2IrO_4

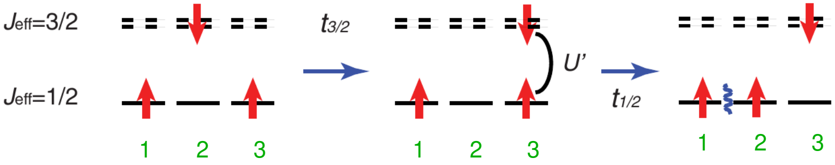

left – a exciton created by RIXS leaves a hole the $J_{eff} = \frac{3}{2}$ state on site 2

center – the hole in the $J_{eff} = \frac{3}{2}$ state hops to site 3

right – the hole in the $J_{eff} = \frac{1}{2}$ state on site 3 hops to site 2, completing the exciton hopping process and creating a magnon

"Magnetic excitation spectra of Sr_2IrO_4 probed by resonant inelastic x-ray scattering: Establishing links to cuprate superconductors," J. Kim, D. Casa, M.H. Upton, T. Gog, Y.-J. Kim, J.F. Mitchell, M. van Veenendaal, M. Daghofer, J. van den Brink, G. Khaliullin, and B.J. Kim, *Phys. Rev. Lett.* **108**, 177003 (2012).